IEEE Access
Multidisciplinary | Rapid Review | Open Access Journal

Received May 11, 2019, accepted June 4, 2019, date of publication July 8, 2019, date of current version August 1, 2019.

Digital Object Identifier 10.1109/ACCESS.2019.2927387

Locating Smartphones Indoors Using Built-In Sensors and Wi-Fi Ranging With an Enhanced Particle Filter

SHIHAO XU[1], RUIZHI CHEN[1,2], YUE YU[1], GUANGYI GUO[1], AND LIXIONG HUANG[1]
[1]State Key Laboratory of Information Engineering in Surveying, Mapping, and Remote Sensing, Wuhan University, Wuhan 430079, China
[2]Collaborative Innovation Center of Geospatial Technology, Wuhan University, Wuhan 430079, China

Corresponding author: Ruizhi Chen (ruizhi.chen@whu.edu.cn)

This work was supported in part by the National Key Research and Development Program of China under Grant 2016YFB0502200 and Grant 2016YFB0502201, in part by the NSFC under Grant 91638203, and in part by Wuhan University through the National Undergraduate Training Programs for Innovation (Double First-Rate Special Program), under Grant 201910486002.

ABSTRACT Sensors-based and radio frequency (RF)-based indoor localization technology is one of the keys in location-based services. The IEEE 802.11-2016 introduced the Wi-Fi fine timing measurement (FTM) protocol, which provides a new approach for Wi-Fi-based indoor localization. However, Wi-Fi signals are susceptible to complex indoor environments. To improve the positioning accuracy and stability, an enhanced particle filter (PF) with two different state update strategies, a new criterion for divergence monitoring and rapid re-initialization is proposed to integrate the advantages of pedestrian dead reckoning (PDR) and Wi-Fi FTM. In addition, an adaptive tilt compensation is proposed to improve real-time heading estimation of conventional PDR, and the Wi-Fi FTM outliers are detected by displacement estimation of the PDR. The experimental results show that the proposed PF has better localization performance than the single source positioning methods in a typical indoor scenario. The accuracy of final localization is within 1 m in 86.7% of the dynamic cases and the average calculation time is less than 0.5 s when the number of particles is 2000.

INDEX TERMS Wi-Fi FTM, pedestrian dead reckoning, particle filter, multi-sensors, indoor localization.

I. INTRODUCTION

Indoor positioning methods with higher accuracy have been discussed in recent years since they can play pivotal roles in the field of artificial intelligence [1]. Lacking the assistance of the Global Navigation Satellite System (GNSS), radio frequency (RF)-based and sensors-based techniques, such as Bluetooth [2], Wi-Fi [3], vision [4], and inertial positioning [5], have been developed for indoor environments. Micro-Electro-Mechanical Systems (MEMS) provide many small but complete and powerful sensors, such as accelerometers, gyroscopes, and magnetometers, that can be used to achieve pedestrian dead reckoning (PDR). PDR is an inertial navigation technology that relies on an inertial measurement unit (IMU) in which an accelerometer can determine travelled distance by integration and a gyroscope and magnetometer can provide heading change and absolute heading, respectively [6]. The current position can then be estimated based on the real-time heading, step-length, and previous position. There are many different IMU deployment methods such as handheld [7], hip-mounted [8], leg-mounted [9], and foot-mounted [10]. Because of the wide range of sensors built into smartphones, they are suitable for use in PDR. However, PDR can only give relative positioning results; small deviations can accumulate over time and make the results unusable. Therefore, it is necessary to introduce absolute positioning methods such as Wi-Fi.

Several main characteristics based on Wi-Fi can be taken advantage of for indoor localization such as time of arrival (TOA) [11], received signal strength indication (RSSI) [12], and channel state information (CSI) [13]. The most common Wi-Fi-based positioning systems use RSSI measurements such as the path-loss model [14] and fingerprinting [15]. Due to complex and changeable indoor scenarios, this method is subject to limitations in accuracy and deployment cost. Another important reference for Wi-Fi positioning methods is the TOA. Accurate time-delay estimation produces a precise range measurement. The 802.11 working group has pro-

The associate editor coordinating the review of this manuscript and approving it for publication was Celimuge Wu.

posed the TOF protocol to improve the time resolution [16], which achieves a time granularity at the microsecond level; however, this is not sufficient for indoor localization. Other technologies, such as ultra-wide band (UWB), are applied to estimate channel responses to acquire a time resolution of sub-nanosecond [17]. In the latest 802.11ac standard [18] an improved TOF protocol called Fine Timing Measurement (FTM) has been introduced, which measures the round-trip-time (RTT) between transmitter and receiver at the same time resolution as UWB by the exchange of frames and the compensation of hardware latency. FTM achieves a ranging accuracy at the meter or even submeter level without any additional infrastructure [19]. We built a complete system to capture the signal described above in which the hardware part follows [20] and the software part is based on the API of Android P [21]. Despite Wi-Fi FTM having a relatively high precision, it suffers from problems such as non-line-of-sight (NLOS) reception [22] and multipath interference, which are difficult to directly solve from the time domain.

Based on a single positioning source, localization typically faces many limitations. The multi-source fusion positioning method integrates various advantages of the single methods and achieves higher positioning accuracy and stability. Filter theory usually becomes the adopted approach to fuse different data. Although Kalman filters (KF) have been widely used, it is hard to find an analytical solution for a highly nonlinear model. Extended Kalman filters (EKF) [17], [23], [24], Unscented Kalman filters (UKF) [15], [25], [26], Bayesian filters (BF) [24], and Monte Carlo simulation (MC) [27] can be applied to solve nonlinear problems. However, EKF adopts the Taylor first-order expansion of the nonlinear model and UKF adopts only a few sigma points to approximate the probability density distribution, and both have limitations in accuracy. Therefore, in this study a particle filter (PF) having higher precision based on Bayesian statistical analysis and Monte Carlo simulation is selected [28]. The filter estimates the probability distribution by the statistical properties of a set of samples called particles. The particles are first sampled from a uniform distribution, and each of them has a state that includes position and weight. At each time, each particle updates position according to PDR information. Wi-Fi FTM measurements are then used to update the weights. The final position estimation can be calculated by averaging the weighted particle set.

In this study, we propose an enhanced particle filter that fuses smartphone built-in sensors, Wi-Fi FTM ranging, and simple map constraints to achieve fast and accurate indoor localization. In summary, the major contributions of this work are as follows:

- We add an adaptive tilt compensation to the conventional PDR algorithm, which can give a real-time and more accurate azimuth estimation for smartphone pitches from 0° to 90°.
- We give solutions to two different strategies to update the particle set state based on two different pedestrian locomotion activities. Then, a new criterion based on Wi-Fi FTM outlier detection and the improved weighted mean-square error (wMSE) method is proposed to judge whether the particle set diverges. To decrease the calculation time, we adopt a rapid re-initialization method from the previous posterior distribution under the static mode.
- We applied an enhanced PF algorithm on indoor localization that combines multi-sensors, Wi-Fi FTM, and simple map information. Implemented experiments demonstrate that the proposed PF algorithm achieves higher accuracy and stability that are not greatly affected by the PDR deviation and the Wi-Fi FTM outliers.

The remainder of the paper is organized as follows: Section II presents some existing work on Wi-Fi FTM and related fusion technologies. Section III describes how the IMU sensors and Wi-Fi FTM are used for indoor pedestrian positioning and presents an enhanced particle filter to fuse PDR and Wi-Fi FTM based on smartphones. In Section IV the experimental setup and results are demonstrated and Section V concludes the paper and points out future work.

II. RELATED WORK

The Wi-Fi FTM protocol was developed from the time-of-flight (TOF) protocol, in which the basic concept is to determine distances by measuring TOA [16]. In 2013, a research team from Intel began to pay attention to the development of this field. This team systematically studied Wi-Fi FTM from the aspects of protocol, fusion algorithms and machine learning algorithm, and has achieved good results. In [16], they introduced how the TOF protocol works in detail and conducted experiments consisting of both ray tracing simulation and real-life tests in an office environment. To reduce the negative impacts on unsynchronized time signal and multipath, they used EKF to fuse TOF measurements with IMU to enhance the performance of TOF system [17]. Then, in 2016 the 802.11 working group standardized the FTM protocol, which allowed the same team to display more convenient research. This time, they compared the positioning performance of KF and BF based on fusing Wi-Fi FTM and map information [19]. Due to the highly nonlinear measurement model, BF was suggested for use. Then, the team proposed a new protocol called collaborative time of arrival (CTOA), which allows the access point (AP) to periodically broadcast a unique beacon [23]. Based on the time of departure (TOD), the TOA and the MAC address recorded in the tag, neighbor clients can measure the distance from the AP and track their locations. Since this mode suffered from a time-tracking challenge, maximum-likelihood estimates (MLEs) in the absence of clock drifts and an EKF model under clock drifts were derived to correct the bias [24]. Their final system achieved a positioning accuracy better than 2 m in 95% of real cases. Moreover, they shared a reference positioning engine and a time-delay measurement database for developing and evaluating the localization system based on Wi-Fi FTM [20]. Dvorecki *et al.* [29] from this team adopted a ''Siamese'' artificial neural network (ANN), based

on the machine learning approach, that aimed at the problem of the inability to separate signals spaced closer than the resolution limited by the signal bandwidth to improve the ranging precision of Wi-Fi FTM. The indoor channel simulation was used to train the model and the real-channel measurements were used to analyze the performance of the ANN and MLEs methods; the results showed that the former outperformed the latter.

To apply Wi-Fi FTM, a specific configuring environment is needed first. Ibrahim [20] *et al.* from Rutgers University proposed a complete open hardware and software platform, including a signal transmitter based on the Intel Dual Band Wireless-AC8260 and a test tool built in Linux. They also studied the key factors and parameters that affect the ranging performance. The indoor experimental results showed that the ranging accuracy reached 2.5 m and the positioning accuracy reached 4 m. Wide applications of Wi-Fi FTM, such as indoor and outdoor vehicle location, have also been studied. Niesen *et al.* [30] proposed an improved dedicated short-range communication method by Wi-Fi FTM to perform outdoor inter-vehicle ranging. A timestamp compression method that discards the most significant bits of each FTM frame has been discussed. Differently from [30], Neri [31] presented an architecture of mileage estimation in indoor vehicle localization. The idea of deploying a Wi-Fi unit on board and placing at least 3 Wi-Fi beacons with the real/virtual track constraint was confirmed to be able to track the noise and clock drift. Monte Carlo simulation was used to analyze the most suitable interval for Wi-Fi beacon deployment to reduce the material consumption. Other fusion method combined with multi-sensors and Wi-Fi FTM, such as UKF, was studied in Yue *et al.* [25]. They proposed a real-time ranging model that reduces the impacts of clock deviation, NLOS, and multipath. With such a ranging model and a robust PDR algorithm, UKF was introduced to fuse these data and gave a final positioning error within 2 m.

Compared with PDR and other Wi-Fi-based localization technologies, Wi-Fi FTM is a relatively new method. Because of its high accuracy and no requirement for additional infrastructure deployment, Wi-Fi FTM will receive much attention in the near future.

III. THEORIES AND METHODS

A. PDR WITH ADAPTIVE TILT COMPENSATION BASED ON SMARTPHONE BUILT-IN SENSORS

Any discussion about localization becomes meaningful only within a certain coordinate framework. In PDR, navigation frame and body frame are involved. The navigation frame is defined as an absolute reference frame and the body frame is defined with the screen of the phone and its default orientation [7]. The body frame uses the right-hand Cartesian coordinate system [6]. Then, a coordinate transformation with Euler angles for pitch, roll and yaw that indicate the rotation around the x, y and z-axes, respectively, is performed to describe how a vector is converted from the navigation frame to the body frame, as shown in Fig. 1.

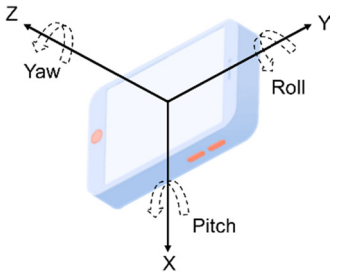

FIGURE 1. Body frame of smartphone and three Euler angles.

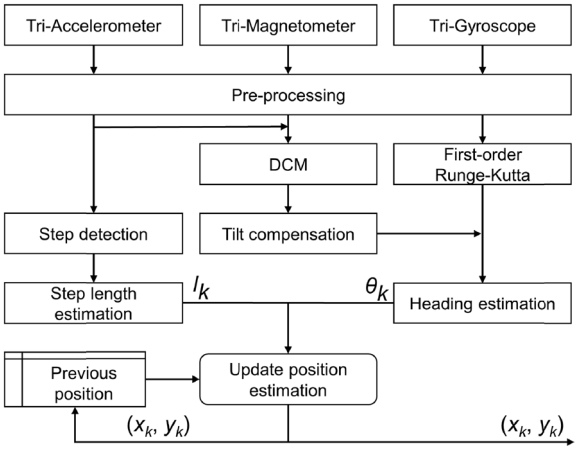

FIGURE 2. Framework of proposed PDR with adaptive tilt compensation.

Based on the definition of coordinate frames and coordinate transformation, the framework of the PDR with adaptive tilt compensation based on smartphones is illustrated in Fig. 2.

1) STEP DETECTION AND STEP-LENGTH ESTIMATION

When a pedestrian walks at a normal speed, his/her center of gravity has a periodic change that allows an accelerometer to record and distinguish steps.

Therefore, several approaches have been proposed to detect steps, including peak detection [32], zero-crossing [33], and autocorrelation [15]. The peak detection approach is adopted in our PDR algorithm. Whether a pedestrian is in a static or walking state can be judged based on the output changes of the accelerometer in the z-axis. Due to inevitable inertia and minor jitter, a low pass filter can be used to smooth the accelerometer outputs and improve the accuracy of step detection [34].

First, the raw data are normalized and the gravity is separated to obtain the pedestrian acceleration:

$$a_p^t = \sqrt{a_x^{t2} + a_y^{t2} + a_z^{t2}} - g \tag{1}$$

where t is the sample timestamp, a_p^t is the pedestrian acceleration, a_x^t, a_y^t, a_z^t indicate the raw accelerometer outputs, and g is the measured value of local gravity acceleration. Since a smartphone's built-in sensors are commonly low-cost and usually have many unwanted noise [6], pseudo peaks will frequently appear. The normalized data can be low-pass filtered

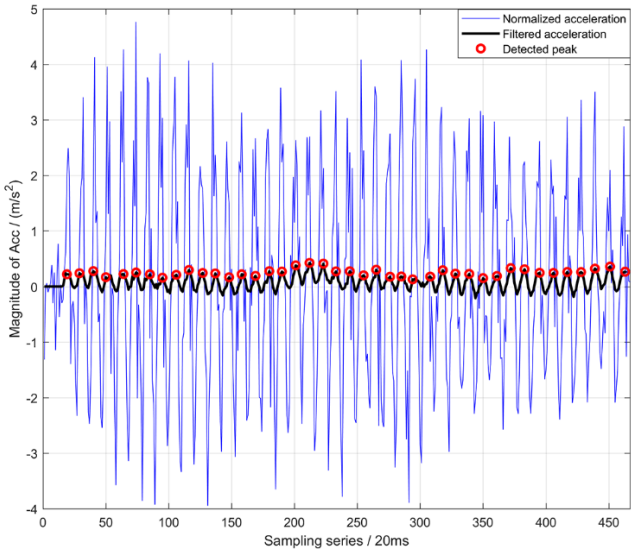

FIGURE 3. Peak detection by accelerometer for 42 counted steps.

with a moving average filter to remove the high frequency perturbations [8], which makes the data smoother:

$$a_{step}^{t} = \frac{1}{N} \sum_{i=t-N+1}^{t} a_{p}^{i} \tag{2}$$

where a_{step}^{t} is the filtered value and N is the sliding window length of the filter, which is a critical factor; in this study $N = 30$. When the filtering process is complete, a time threshold is set to further eliminate pseudo-peak residuals. According to [15], the stride frequency of normal walking ranges from 1 to 2.5 Hz, and the minimum threshold is thus set to 0.4 s. If the determined interval between two consecutive adjacent peaks is less than this threshold, one of those peaks will be rejected, such that:

$$\Delta T = t_{step}^{n+1} - t_{step}^{n} > \Delta T_{threshold} \tag{3}$$

where n is the number of adjacent peaks. Fig. 3 shows the result of step detection; the 42 steps counted are marked with red circles.

The accelerometer also participates in step-length estimation. In addition to being closely related to the step frequency, the step length is also affected by the pedestrian's height, weight and walking habits. Therefore, there is not a completely universal step length estimation model at the moment. Many approaches have been proposed such as linear models [6], [35], [36], nonlinear models [32], and adaptive models [5], [10]. In this study, the length of each step is estimated using a linear model [35]:

$$SL = [0.7 + a\,(H - 1.75) + b\frac{(SF - 1.79)H}{1.75}]c \tag{4}$$

where SL is the estimated step length, SF is the real-time step frequency defined by the time interval between two consecutive adjacent step peaks that are estimated by the accelerometer, and H is the pedestrian height, which should be preset. a, b, and c are the parameters of the model [35], which are $a = 0.371$, $b = 0.227$, and $c = 1$. This is an empirical model and can be directly used without any training samples. Every parameter is simple and the only one of concern is the pedestrian height.

Based on the adopted step detection and step-length estimation methods, a verification was took in a long straight corridor (48.05 m). The tester walked three round trips holding the smartphone, and the estimated distance was compared to the actual, results show a total error rate of less than 3%.

2) HEADING ESTIMATION

Heading estimation is pivotal to the entire PDR approach. With different combinations of IMU sensors, there are many approaches to obtain heading estimates, such as quaternion based on gyroscopes [37], digital compass based on accelerometers and magnetometers [6], [10], the direction cosine matrix (DCM) [38], [39], and EKF fusion [40]. In general, smartphones can obtain an absolute direction from magnetometers as well as a relative direction from gyroscopes. However, magnetometers can be seriously disturbed indoors and give unstable outputs. Therefore, quaternion based on a gyroscope are adopted here to estimate headings.

Quaternion, 4×1 unit-norm vectors in $\mathbb{R}^4$ [41], can be used to describe certain rotation processes. Given an original vector $\boldsymbol{a}$ and a rotation action $\boldsymbol{q}$ under the body frame, the rotated vector $\boldsymbol{a}'$ can be expressed as:

$$\boldsymbol{a}' = \boldsymbol{q}\boldsymbol{a}\boldsymbol{q}^{*} \tag{5}$$

where $\boldsymbol{q} = a + b\boldsymbol{i} + c\boldsymbol{j} + d\boldsymbol{k}$, for which $\boldsymbol{i}, \boldsymbol{j}, \boldsymbol{k}$ are imaginary units, a to d are real numbers, and $\boldsymbol{q}^{*}$ is the inverse of $\boldsymbol{q}$. The quaternion must be constantly updated to obtain the real-time rotation result relative to the initial state, which can be expressed as:

$$\boldsymbol{q}_{t+1} = \boldsymbol{q}_{t} + \Delta T \dot{\boldsymbol{q}}_{t} \tag{6}$$

where $\dot{\boldsymbol{q}}_{t}$ is an ordinary differential equation that can be written as:

$$\dot{\boldsymbol{q}}_{t} = \frac{1}{2}\boldsymbol{\Omega}(\boldsymbol{\omega})\boldsymbol{q}_{t} \tag{7}$$

where $\Omega(\boldsymbol{\omega})$ is a matrix consisting of the gyroscope outputs. The first order Runge–Kutta method is then used to solve for the $\dot{q}_{t}$, and the final updated quaternion is written as follows:

$$\boldsymbol{q}_{t+1} = \boldsymbol{q}_{t} + \frac{\Delta T}{2}\begin{bmatrix} 0 & -\omega_x & -\omega_y & -\omega_z \\ \omega_x & 0 & \omega_z & -\omega_y \\ \omega_y & -\omega_z & 0 & \omega_x \\ \omega_z & \omega_y & -\omega_x & 0 \end{bmatrix}\boldsymbol{q}_{t} \tag{8}$$

where ΔT is the sampling interval of the gyroscope and ω_x, ω_y, ω_z are the moving average filtered outputs of the gyroscope, with a sliding window length of 15. Assuming that the quaternion corresponding to the initial orientation of the horizontal smartphone is (1, 0, 0, 0), the rotation matrix of

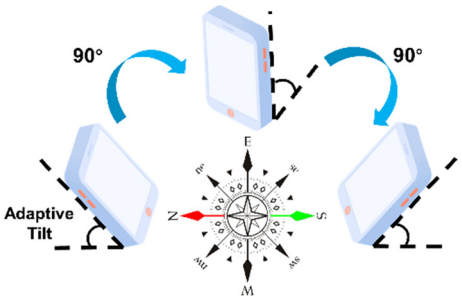

FIGURE 4. Heading changes from 0° to 180° when tilt angle is adaptive.

the body frame with respect to the navigation frame at any timestamp can then be expressed as:

$$\boldsymbol{T}_{N_t}^{B} = \begin{bmatrix} 1-2c^2-2d^2 & 2bc+2ad & 2bd-2ac \\ 2bc-2ad & 1-2b^2-2d^2 & 2ab+2cd \\ 2ac+2bd & 2cd-2ab & 1-2b^2-2c^2 \end{bmatrix}_t \quad (9)$$

where $\boldsymbol{T}_{N_t}^{B}$ is the DCM that transforms vectors from the navigation frame to the body frame at timestamp t. a to d are given in terms of $\boldsymbol{q}_{t+1}$. To correct the integration error and the quantization error of the gyroscope, a numerical error correction approach is performed as in [39]. Finally, the real-time heading relative to the given initial orientation is calculated from (10):

$$\theta = arctan(\frac{2bc+2ad}{1-2b^2-2d^2}) \quad (10)$$

3) ADAPTIVE TILT COMPENSATION

Regarding tilt compensation in PDR, it is common to correct the bias of a magnetometer with an accelerometer and obtain heading outputs from the latter [10], [42], [43]. The tilt refers to the angle between the horizontal plane of the navigation frame and the screen plane of the smartphone gripped naturally by pedestrians. What we explored is how a big tilt would bring a negative impact to conventional PDR when the range of pitch is between 0° and 90° since the heading estimation algorithm given in previous section could not work effectively under the circumstance illustrated in Fig. 4.

When the phone is not horizontal, the gyroscope outputs can only represent the rotation relative to its initial state under the body frame. Because the angular velocity of the z-axis has taken most of the contribution to integration when the phone is horizontal, whereas only part of the gyroscope outputs are doing the same thing now, the result obtained from the abovementioned heading estimation method always diverges greatly from the actual value. Therefore, a DCM calculated by an accelerometer and magnetometer is applied to generate the tilt compensation approach.

The DCM is written in terms of the rotation matrix that describes the orientation transformation of two different coordinate reference frames. According to the Android API [44], the rotation matrix $\boldsymbol{C}_B^N$ transforming a vector from the body frame to the navigation frame can be directly calculated as follows:

$$\boldsymbol{C}_B^N = \begin{bmatrix} H_x & H_y & H_z \\ M_x & M_y & M_z \\ A_x & A_y & A_z \end{bmatrix} \quad (11)$$

where $\boldsymbol{H}$, $\boldsymbol{M}$, and $\boldsymbol{A}$ are associated with the sensor outputs; details can be found in [44]. In general, (11) can be used directly as a DCM. However, the only parameter we care about is the pitch, and the heading has been solved by the quaternion, which means that yaw and roll are redundant here. Therefore, only the pitch is obtained from $\boldsymbol{C}_B^N$:

$$p = arcsin(-A_y) \quad (12)$$

Then, a new DCM is calculated as:

$$DCM = \begin{bmatrix} 1 & 0 & 0 \\ 0 & C_p & S_p \\ 0 & -S_p & C_p \end{bmatrix} \quad (13)$$

where C is cosine and S is sine. Next, two rotation matrixes are combined to obtain a tilt compensated matrix:

$$\boldsymbol{R}_{tilt} = DCM \cdot \boldsymbol{T}_N^B \quad (14)$$

where $\boldsymbol{T}_N^B$ is obtained from (9). Finally, the tilt-compensated and real-time heading is calculated as:

$$\theta_{tilt-compensated} = arctan(\frac{R_{12}}{R_{22}}) \quad (15)$$

where R_{12} is the element in row 1 and column 2 and R_{22} is the element in row 2 and column 2 of $\boldsymbol{R}_{tilt}$.

B. ANALYSIS OF WI-FI FTM RANGING

1) RANGING MODEL

Wi-Fi FTM allows a smartphone (iSTA in the following) to determine distances with multiple APs (rSTA in the following) at the same time by an exchange of multiple FTM frames. With reference to the standard [18], a complete FTM session can be described as follows.

First, the iSTA should send an initial FTM request frame to the rSTA to ensure that no communication conflicts occur. Then, the rSTA will transmit an initial FTM frame within 10 ms as a response indicating that the negotiation was complete. To avoid completely saturating either the network capacity or the processing capacity of the single STA [31], the burst instance mechanism is applied during the measurement exchange phase. The interval between two consecutive burst instances should be longer than 0.1 ms, in units of 100 ms. A new burst will be triggered by an FTM request according to the iSTA. Next, the rSTA will record TOD t_1^1 of the first FTM frame, and the iSTA then measures TOA t_2^1 of the signal and TOD t_3^1 of the ACK frame. TOA t_4^1 is then captured by the rSTA, and the timestamps t_1^1 and t_4^1 will be posted to iSTA in the next FTM frame to calculate the RTT. There can be multiple FTM frames in a burst, and the interval of each consecutive FTM frames should be longer than 0.1 ms and shorter than 25.6 ms, in units of 100 μs. The entire procedure is illustrated in Fig. 5.

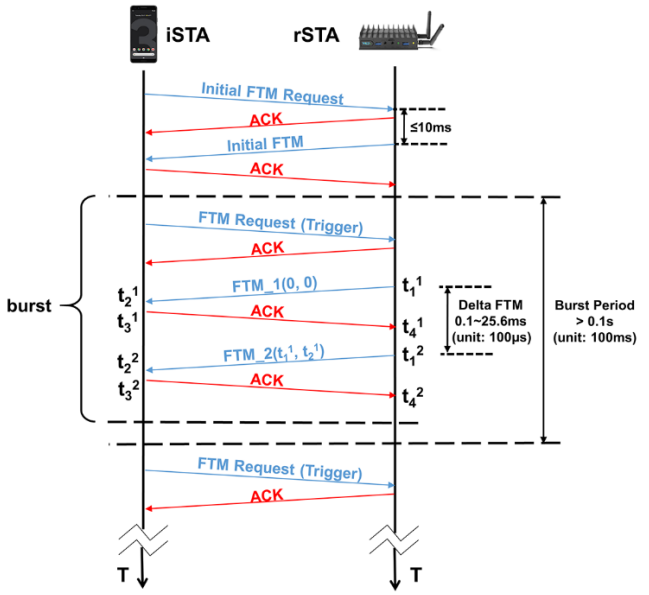

FIGURE 5. Procedure of Wi-Fi FTM; FTMs per burst = 2.

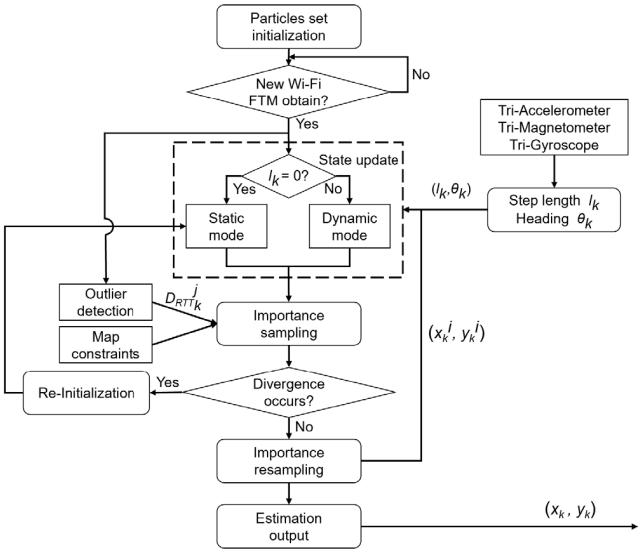

FIGURE 6. Framework of proposed PF.

Finally, the mean distance between iSTA and rSTA within one burst can be calculated by (16):

$$D_{RTT} = \frac{c}{2n}\sum_{k=1}^{n}\left(t_4^k - t_1^k\right) - \left(t_3^k - t_2^k\right) \tag{16}$$

where c is the speed of light and n is the number of FTM frames within a burst instance. Then, the least squares (LS) algorithm can be used to obtain a real-time 2D position from at least three different APs:

$$\begin{aligned} \boldsymbol{X} &= \left(\boldsymbol{A}^T\boldsymbol{A}\right)^{-1}\boldsymbol{A}^T\boldsymbol{L} \\ \boldsymbol{A} &= 2\begin{bmatrix} (x_1 - x_2) & (y_1 - y_2) \\ (x_1 - x_3) & (y_1 - y_3) \\ \vdots & \vdots \\ (x_1 - x_j) & (y_1 - y_j) \end{bmatrix} \\ \boldsymbol{L} &= \begin{bmatrix} D_{RTT}^{22} - D_{RTT}^{12} - \left(x_2^2 - x_1^2\right) - \left(y_2^2 - y_1^2\right) \\ D_{RTT}^{32} - D_{RTT}^{12} - \left(x_3^2 - x_1^2\right) - \left(y_3^2 - y_1^2\right) \\ \vdots \\ D_{RTT}^{j2} - D_{RTT}^{12} - \left(x_j^2 - x_1^2\right) - \left(y_j^2 - y_1^2\right) \end{bmatrix} \end{aligned} \tag{17}$$

where $\boldsymbol{X}$ is the position estimation, $\boldsymbol{X} = (x, y)$, j is the number of APs, x_j and y_j are the positions of the j-th AP, and D_{RTT}^j is the distance estimation result from the j-th AP.

2) OUTLIER DETECTION

Because the multipath and NLOS problems cause the distances to be overestimated or underestimated, indoor environments are challenging for time-based ranging systems [20], [25]. One way to detect these outliers based on spatial relations is to use IMU sensors. As a pedestrian moves from a previous position to a current position, the amount of the change in distance between the pedestrian and the AP is limited. Assuming the previous and the current distance estimations d_{pre}, d_{cur} are both known and without errors, an ideal relationship can then be described as:

$$\left|d_{cur} - d_{pre}\right| = d_s \tag{18}$$

where d_s is the displacement estimated by PDR. However, the outputs of Wi-Fi FTM fluctuate around the true value under normal conditions, which can make current displacement to be overestimated or underestimated. To make equation (18) more robust, it can be modified as follows:

$$\left|d_{cur} - d_{pre}\right| \le \eta d_s \tag{19}$$

where η is the coefficient to limit the outliers, which can be determined by experiments. A new measurement can be considered as an outlier if it does not satisfy (19). Then, the detected outlier will be replaced by a temporary variable d_{temp} for comparison with the next distance estimation, with d_{temp} assigned as follows:

$$d_{temp} = \begin{cases} d_{pre} + d_s d_{cur} > d_{pre} + \eta d_s \\ d_{pre} - d_s d_{cur} < d_{pre} - \eta d_s \end{cases} \tag{20}$$

Note that the temporary variable only works during the outlier detection phase and would not affect the specific position estimation.

C. ENHANCED PARTICLE FILTER ALGORITHM BASED ON SMARTPHONES

In this section, we propose an enhanced PF to fuse PDR measurements, Wi-Fi FTM measurements and some simple map constraints. In this algorithm, two different update strategies for particle set, a criterion of divergence monitoring that considers the characteristics of Wi-Fi FTM, and a rapid re-initialization method are applied. The framework of the proposed PF is illustrated in Fig. 6.

1) NONLINEAR FILTER BASED ON THE BAYESIAN APPROACH AND THE MONTE CARLO METHOD

A Bayesian approach to nonlinear filtering offers a systematic way to combine all prior knowledge of known states, modeling assumptions, and observation information to approximate the posterior probability density function (pdf) of the system state [27], [45], [46]. In general, a dynamic system can be described by a state model and an observation model as follows:

$$\begin{cases} \boldsymbol{X}_k = f_k\left(\boldsymbol{X}_{k-1}, \boldsymbol{W}_k\right) & \boldsymbol{W}_k \sim N\left(0, \boldsymbol{Q}_k\right) \\ \boldsymbol{Z}_k = h_k\left(\boldsymbol{X}_k, \boldsymbol{V}_k\right) & \boldsymbol{V}_k \sim N\left(0, \boldsymbol{R}_k\right) \end{cases} \tag{21}$$

where $\boldsymbol{X}_k \in \mathbb{R}^{n_x}$ and $\boldsymbol{Z}_k \in \mathbb{R}^{n_z}$ are the system state and observation at timestamp k, and $\boldsymbol{X}_{k-1}$ is the state at *k-1*. $\boldsymbol{W}_k \in \mathbb{R}^{n_w}$ and $\boldsymbol{V}_k \in \mathbb{R}^{n_v}$ are the process noise and the measurement noise, which are generally assumed to be a Gaussian noise with null mean and covariance matrix $\boldsymbol{Q}_k$ and $\boldsymbol{R}_k$, respectively. f_k:$\mathbb{R}^{n_x} \times \mathbb{R}^{n_w} \rightarrow \mathbb{R}^{n_x}$ is a nonlinear function that reflects the relationship between the current and the previous state. h_k:$\mathbb{R}^{n_x} \times \mathbb{R}^{n_v} \rightarrow \mathbb{R}^{n_z}$ expresses the relationship between the observations and the states. To obtain an optimal estimation by determining the belief of different state variables, the posterior pdf $\mathrm{p}(\boldsymbol{X}_k|\boldsymbol{Z}_{1:k})$ is needed. First, it is assumed that the state transition obeys the Markov process of order one, which is $\mathrm{p}(\boldsymbol{X}_k|\boldsymbol{X}_{0:k-1}) = \mathrm{p}(\boldsymbol{X}_k|\boldsymbol{X}_{k-1})$. If a sequence of observations are available at timestamp k, then the updated prior pdf can be calculated by:

$$\begin{aligned} & p\left(\boldsymbol{X}_{\boldsymbol{k}} \mid \boldsymbol{Z}_{1:k-1}\right) \\ &= \int p(\boldsymbol{X}_k, \boldsymbol{X}_{k-1}|\boldsymbol{Z}_{1:k-1}) d\boldsymbol{X}_{k-1} \\ &= \int p(\boldsymbol{X}_k|\boldsymbol{X}_{k-1}, \boldsymbol{Z}_{1:k-1}) p(\boldsymbol{X}_{k-1}|\boldsymbol{Z}_{1:k-1}) d\boldsymbol{X}_{k-1} \\ &= \int p(\boldsymbol{X}_k|\boldsymbol{X}_{k-1}) p(\boldsymbol{X}_{k-1}|\boldsymbol{Z}_{1:k-1}) d\boldsymbol{X}_{k-1} \end{aligned} \tag{22}$$

where the transition probability distribution $p(\boldsymbol{X}_k|\boldsymbol{X}_{k-1})$ is defined by $\boldsymbol{X}_k$ in (21) and the previous posterior $p(\boldsymbol{X}_{k-1}|\boldsymbol{Z}_{1:k-1})$ is assumed to be known. Then, the current posterior pdf can be calculated by:

$$\begin{aligned} p(\boldsymbol{X}_k|\boldsymbol{Z}_{1:k}) &= \frac{p(\boldsymbol{Z}_k|\boldsymbol{X}_k, \boldsymbol{Z}_{1:k-1}) p(\boldsymbol{X}_k|\boldsymbol{Z}_{1:k-1})}{p(\boldsymbol{Z}_k|\boldsymbol{Z}_{1:k-1})} \\ &= \frac{p(\boldsymbol{Z}_k|\boldsymbol{X}_k) p(\boldsymbol{X}_k|\boldsymbol{Z}_{1:k-1})}{p(\boldsymbol{Z}_k|\boldsymbol{Z}_{1:k-1})} \end{aligned} \tag{23}$$

where the $p(\boldsymbol{Z}_k|\boldsymbol{Z}_{1:k-1})$ is the normalizing constant:

$$p(\boldsymbol{Z}_k|\boldsymbol{Z}_{1:k-1}) = \int p(\boldsymbol{Z}_k|\boldsymbol{X}_k) p(\boldsymbol{X}_k|\boldsymbol{Z}_{1:k-1}) d\boldsymbol{X}_k \tag{24}$$

where the $p(\boldsymbol{Z}_k|\boldsymbol{X}_k)$ is the likelihood function defined by $\boldsymbol{Z}_k$ in (21).

Due to the complex integral operation involved in (22) and (24), it is difficult to solve such a pdf problem when the system model is nonlinear [46]. The Monte Carlo method provides an approach to suboptimal estimation by approximation. By finding a set of weighted and random MC samples in the state space to represent the posterior pdf, the mean of this sample set could be substituted for the integration to obtain results. From the above analysis, it is assumed that N weighted samples can be obtained from the true posterior probability. On one hand, the weight is initialized to $\frac{1}{N}$ and updated by:

$$w_k^i \propto w_{k-1}^i \frac{p(\boldsymbol{Z}_k|\boldsymbol{X}_k^i) p(\boldsymbol{X}_k^i|\boldsymbol{X}_{k-1}^i)}{q(\boldsymbol{X}_k^i|\boldsymbol{X}_{k-1}^i, \boldsymbol{Z}_k)} \tag{25}$$

where $q(\cdot)$ is the importance density. On the other hand, the approximate posterior pdf can be calculated as:

$$p(\boldsymbol{X}_k|\boldsymbol{Z}_{1:k}) \approx \sum_{i=1}^{N} w_k^i \delta(\boldsymbol{X}_k - \boldsymbol{X}_k^i) \tag{26}$$

where w_k^i and $\boldsymbol{X}_k^i$ are the weight and the state of the i-th sample, respectively, and $\delta(\cdot)$ is the Dirac delta function. When $N \rightarrow \infty$, the approximation approaches the true posterior density [46].

2) DIFFERENT STRATEGIES DURING THE STATE UPDATE PHASE BASED ON TWO LOCOMOTION MODES

In this study, the state vector consists of 2-dimensional position (x, y) and heading θ(in degrees):

$$\boldsymbol{X}_k = \begin{bmatrix} \theta_k \\ x_k \\ y_k \end{bmatrix}$$

The number of samples is assumed to be N. In the initial phase, each MC sample, called a particle, is generated from the initial probability distribution $p(\boldsymbol{X}_0)$ with equal weights [28]. Applying the LS method, four Wi-Fi FTM measurements provide the initial position for the particle set. The initial heading of each particle is drawn from the uniform distribution $U(0, 2\pi)$. After initialization, two different strategies for state update are deployed when a new group of Wi-Fi FTM measurements is received.

In the Bayesian approach, the particle set states are updated from the prespecified proposal distribution $q(\cdot)$. The closer the proposed $q(\cdot)$ is to the posterior distribution, the closer the particle set is to the true value. A typical selection for $q(\cdot)$ is the transition probability distribution $p(\boldsymbol{X}_k|\boldsymbol{X}_{k-1})$, which had only been applied as one form in some past works, some of which assumed that the process noise obeys a Gaussian distribution [47], [48], whereas the other one assumed that the noise obeys the Student's t distribution [28]. To achieve better accuracy and adaptability, we combine these ideas with the characteristics of PDR and Wi-Fi FTM and divide pedestrian navigation into static and dynamic modes.

- Static mode

If the displacement estimation of the PDR is 0, the state transition model at timestamp k of the i-th particle is then described as:

$$\begin{bmatrix} \hat{\theta}_k^i \\ \hat{x}_k^i \\ \hat{y}_k^i \end{bmatrix} = \begin{bmatrix} \theta_{k-1}^i + \delta_\theta \\ x_{k-1}^i + \delta_l sin(\hat{\theta}_k^i) \\ y_{k-1}^i + \delta_l cos(\hat{\theta}_k^i) \end{bmatrix} \tag{27}$$

where $\hat{\theta}_k^i$, $\hat{x}_k^i$, $\hat{y}_k^i$ are the updated state vector, θ_{k-1}^i, x_{k-1}^i, y_{k-1}^i are previous estimation outputs, and δ_θ and δ_l indicate the uncertainty of heading change and displacement, respectively, both of which are Gaussian noise with null means and variances σ_θ^2 and σ_l^2, respectively. These variances are significant to the performance of the filter in static mode. Assuming that the pedestrian is stationary, the PDR has almost no contribution other than the zero step-length constraint, and the localization thus relies more on Wi-Fi FTM at this moment. According to our test results, the outputs of Wi-Fi FTM in indoor environments fluctuate within a true value of ± 2 m, which means that the position estimation by Wi-Fi FTM falls within a circle with a radius of at least 2 m. In this case, to ensure that all observation-series information is used and that the range of the particle set is sufficiently large to cover the entire interesting state-space area, larger process variances than the actual accuracy of the PDR would indicate are needed [28].

- Dynamic mode

If a footstep is detected at timestamp k, then the state transition model can be modified as follows:

$$\begin{bmatrix} \hat{\theta}_k^i \\ \hat{x}_k^i \\ \hat{y}_k^i \end{bmatrix} = \begin{bmatrix} \theta_{k-1}^i + \Delta\theta_k^i + \delta_\theta \\ x_{k-1}^i + (l_k^i + \delta_l) sin(\hat{\theta}_k^i) \\ y_{k-1}^i + (l_k^i + \delta_l) cos(\hat{\theta}_k^i) \end{bmatrix} \tag{28}$$

where $\Delta\theta_k^i$ is the increment estimation of heading and l_k^i is the displacement estimation by PDR. Differently than for the static mode, we are more willing to believe such definite variables since the PDR is available and reliable over a short period. Therefore, the variances δ_θ and δ_l are set to the actual values.

3) WEIGHT UPDATE WITH MAP CONSTRAINTS AND WI-FI FTM OUTLIER DETECTION

When the state prediction stage is complete, the Wi-Fi FTM measurements are then used for the update stage. PF estimates position by the particle set; however, it is common to mistakes that some particles enter an inaccessible area or take an impossible displacement such as wall collisions [28], [49], [50]. Therefore, a simple map filter is deployed to reject the particles passing through the wall as follows:

$$w_k^i \propto \begin{cases} 0 & rejection\ occured \\ w_{k-1}^i & others \end{cases} \tag{29}$$

For the accepted transitions, the weight is updated according to (25), in which a Gaussian distribution is adopted here:

$$w_k^i = w_{k-1}^i \cdot \exp\left\{ -\frac{\left(\boldsymbol{Z}_k - \boldsymbol{Z}_k^{si}\right)^2}{2\boldsymbol{R}_k} \right\}$$

$$\boldsymbol{Z}_k = \begin{bmatrix} D_{RTT_k}^1 \\ D_{RTT_k}^2 \\ \vdots \\ D_{RTT_k}^j \end{bmatrix}, \boldsymbol{Z}_k^{si} = \begin{bmatrix} \sqrt{(\hat{x}_k^i - x_1)^2 - (\hat{y}_k^i - y_1)^2} \\ \sqrt{(\hat{x}_k^i - x_2)^2 - (\hat{y}_k^i - y_2)^2} \\ \vdots \\ \sqrt{(\hat{x}_k^i - x_j)^2 - (\hat{y}_k^i - y_j)^2} \end{bmatrix} \tag{30}$$

where $\boldsymbol{Z}_k$ is a j-dimensional column vector and describes the observed distances between the current location and each AP, $\boldsymbol{Z}_k^{si} = h_k\left(\hat{\boldsymbol{X}}_k^i\right)$ is an estimated distance vector calculated by the known locations x_j, y_j of the APs and the predicated location of the i-th particle, and $\boldsymbol{R}_k$ is the covariance matrix of observations, written as:

$$\boldsymbol{R}_k = \begin{bmatrix} 0_{RTT_2} & & & \\ & \sigma_{RTT_2}^2 & & \\ & & \ddots & \\ & & & \sigma_{RTT_j}^2 \end{bmatrix} \tag{31}$$

where $\sigma_{RTT_j}^2$ is the variance of the j-th AP measurements. In general, σ_{RTT}^2 is obtained from the actual measured data. However, if a Wi-Fi FTM outlier is detected, the corresponding variance will be set to a very large value. Then, the normalization of all weights is performed by:

$$\tilde{w}_k^i = \frac{w_k^i}{\sum_{i=1}^N w_k^i} \tag{32}$$

4) DIVERGENCE MONITORING AND RAPID RE-INITIALIZATION OF PARTICLE SET

Although the PF performs well most of the time, particle sets could sometimes become invalid when the difference between the likelihood $P(\boldsymbol{Z}_k^s | \boldsymbol{X}_k^{1:N})$ and the observation $\boldsymbol{Z}_k$ is too large or when most of the particles occur in invalid transitions. Different criteria [44], [48], [50] to analyze the divergence as mentioned above, have been discussed in [28], which used the KF as a fallback filter to monitor the quality of the particle cloud. We think it is an extra computational overhead to perform a parallel KF interleaved in time and propose a monitoring criterion with an improved wMSE method.

It is pivotal to detect when the particle set exceeds a normal threshold and deal with the outliers among the observations. Two parts of (30) describe such a difference between a *priori* data and observations, as well as the outliers. The original covariance matrix is used rather than its inverse, which is different from equation (30) and source [49]. Then, twice the RMSE, calculated from a sequence of actual measurements of each AP, is taken as the ranging error threshold. This method is fast and does not require too many computing resources because most preparation work has been completed in the weight update phase. For each particle, the criterion can be expressed as follows:

$$wMSE = \left(\boldsymbol{Z}_k - \boldsymbol{Z}_k^{si}\right)^T \boldsymbol{R}_k \left(\boldsymbol{Z}_k - \boldsymbol{Z}_k^{si}\right) < \xi \tag{33}$$

where ξ is the threshold determined by twice the RMSE of the Wi-Fi FTM ranging and by the $\boldsymbol{R}_k$ without considering outliers. According to the proposed criterion,

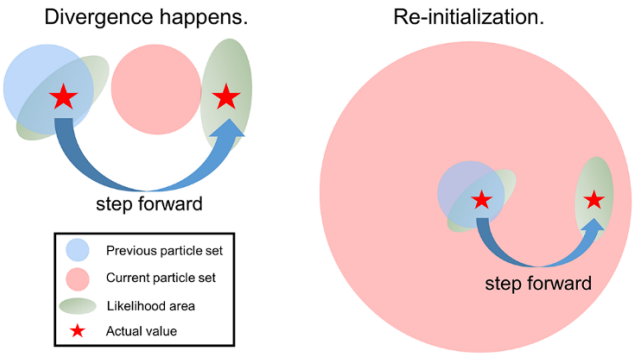

FIGURE 7. Rapid re-initialization from the previous posterior in static mode.

if the calculated error of one particle exceeds the threshold, we regard it as a failed particle. Moreover, if $\lambda\%$ of the particles exceed the threshold, we are confident that divergence occurs; λ is a parameter for which $1 \ll \lambda \leq 100$.

Since the divergence can be a significant computational burden for smartphones, it is necessary to quickly recover the particle set by the operation of re-initialization when the particles become stuck. The general idea is to use a very diffuse prior or to infer external information [45]. However, suitable external information could not easily be found in our system, and we thus re-initialized the particles from the transition probability distribution $p(\boldsymbol{X}_k|\boldsymbol{X}_{k-1})$ under static mode. Once the divergence happens, the filter will recover particles based on the previous posterior $P(\boldsymbol{X}_{k-1}^{1:N})$. Because the static mode can increase the coverage of the particle set more rapidly than the dynamic mode, more particles are moved into the region covered by the likelihood function, which is shown in Fig. 7.

In the case when the divergence does not occur, the PF suffers another problem called sample impoverishment due to particles with low weight disappearing by iteration from the beginning. Different resampling techniques, such as random resampling [45], multinomial resampling [51], and minimum-sampling-variance resampling [52], are used to ensure particle set diversity. Here, we applied a random resampling method with uniform distribution $U(0, 1)$ to select particles, and the selected particle set will become the initial input for the next iteration.

Finally, the position estimation is calculated as the average of weighted particle locations:

$$\begin{cases} x_k = \sum_{i=1}^{N} \tilde{w}_k^i \hat{x}_k^i \\ y_k = \sum_{i=1}^{N} \tilde{w}_k^i \hat{y}_k^i \end{cases} \tag{34}$$

The entire algorithm is summarized as follows:

Algorithm 1 Enhanced Particle Filter Based on Smartphones

1. **Initialization:**
   Perform LS to obtain initial position (x_0, y_0). For each particle $i \in 1, \ldots, N$, set $x_0^i = x_0$, $y_0^i = y_0$, $w_0^i = \frac{1}{N}$, $\theta_0^i \sim U(0, 2\pi)$. Set the time index $k := 1$.
2. **State update:**
   if a new group of Wi-Fi FTM measurements are received
   if no footstep is detected, **then**
   for each particle $i \in 1, \ldots, N$ generate from Static mode of $p(\boldsymbol{X}_k|\boldsymbol{X}_{k-1})$.
   else
   for each particle $i \in 1, \ldots, N$ generate from Dynamic mode of $p(\boldsymbol{X}_k|\boldsymbol{X}_{k-1})$.
   end if
   end if
3. **Weight update:**
   For each particle $i \in 1, \ldots, N$,
   if a wall collision is detected **then**
   $w_k^i \leftarrow 0$.
   else
   according to observations and outlier detection, $w_k^i \propto w_{k-1}^i$.
   end if
   Normalize the weights.
4. **Divergence monitoring and rapid re-initialization:**
   if for $\lambda\%$ of N particles, $wMSE > \xi$ **then**
   perform re-initialization as Static mode of $p(\boldsymbol{X}_k|\boldsymbol{X}_{k-1}) \leftarrow P(\boldsymbol{X}_{k-1}^{1:N})$, and go to Phase 2.
   else
   go to Phase 5.
   end if
5. **Resampling and output:**
   For each particle $i \in 1, \ldots, N$, resampling as $\tilde{w}_k^i \sim U(0, 1)$ & $CDF(\tilde{w}_k^i)$.
   Report the position from weighted particle set $(x_k, y_k) \leftarrow \tilde{w}_k^{1:N}$ & $\hat{X}_k^{1:N}$
   if the localization is end **then**
   stop.
   else
   set $k := k+1$ and go to Phase 2.
   end if

IV. EXPERIMENTAL RESULTS

A. EXPERIMENTAL SETUP

The proposed PF and single source positioning methods were all tested in a typical indoor office scenario in which the size was 11 m $*$ (12.4 m/10 m) $*$ 3 m. A total of 11 check points were set on the scheduled path, and their locations were manually measured using an SNDWAY SW-M80 rangefinder, which can supply each observation with ± 1.5 mm precision. The reference trajectory of one lap for all subsequent experiments was set following the check point order of "4, 5, 11, 10, 9, 8, 7, 6, 5, 11, 10, 9, 1, 2, 3, 4". Our tester is 1.75 m tall, and the Google Pixel 3 smartphone was used in all experiments. Since Wi-Fi FTM is limited by the protocol, its sampling rate was set to 3 Hz, whereas the IMU sensors remained working at 50 Hz in the background. The 2D floor plan of the test environment is shown in Fig. 8.

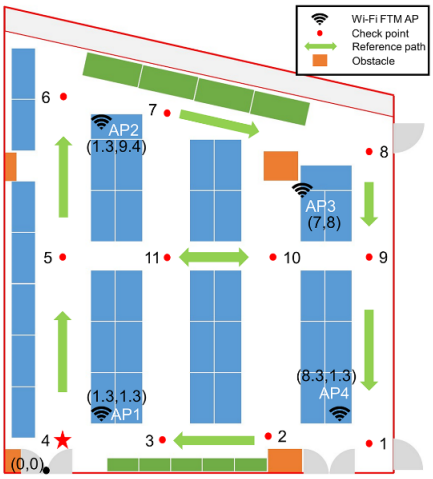

FIGURE 8. 2D floor plan of the test environment.

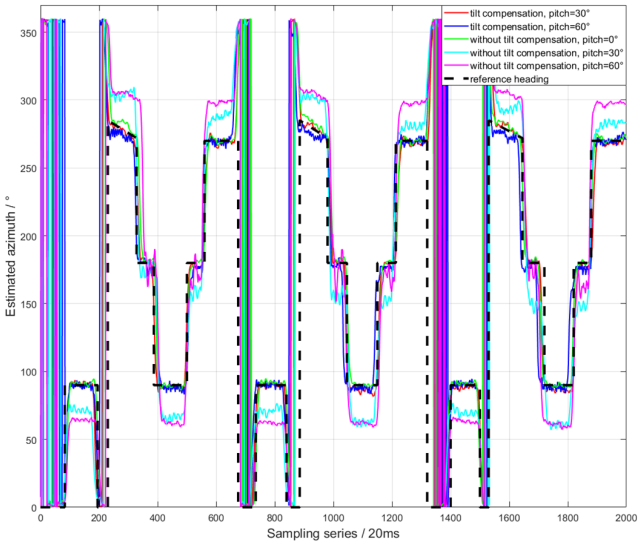

FIGURE 9. Results of comparison experiments in heading estimation.

B. PERFORMANCE EVALUATION OF HEADING ESTIMATION WITH ADAPTIVE TILT COMPENSATION

The performance of adaptive tilt compensation was evaluated in the first experiment. The tester held the phone at different attitudes of pitches 0°, 30°, 60° and walked 12 laps around the office. The initial heading was assumed as 0°. Contrastive experiments were performed as follows:

- Heading estimation when the pitch was 0° with/without tilt compensation.
- Heading estimation when the pitch was 30°/60° with tilt compensation.
- Heading estimation when the pitch was 30°/60° with/without tilt compensation.

Fig. 9 describes the heading estimation under different configurations. It was found that, compared with the reference azimuth, only the results of pitch 30°/60° without tilt compensation had a significant deviation (approximately 30°), whereas others showed good adaptability and accuracy.

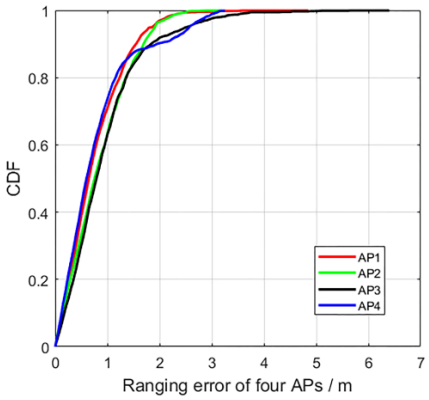

FIGURE 10. Ranging error of four APs.

The second comparison indicated that the tilt compensation could adapt to different pitch angles, and the third comparison found that the tilt compensation does correct the deviation of the conventional PDR when the phone is not horizontal. However, due to more jitters that will affect the phone when it is closer to vertical, the compensation error will sometimes be relatively large (±4°).

C. WI-FI FTM RANGING RESULTS AND ANALYSIS

Analysis of Wi-Fi FTM ranging was conducted in the second experiment. To verify the ranging accuracy of Wi-Fi FTM in the multipath/NLOS mixed indoor scenario, the phone was placed on the first 9 check points at a height of 1.2 m in turn, and each point was tested for 2 minutes to record approximately 200 distance estimations. The true distances were measured using the rangefinder. Next, outlier detection was performed for each AP. We varied the ground distance from 10 m to 0 m with steps of 0.6 m. The real-time distance and step-length estimates were recorded, and the corresponding monitoring state was set to 1 if the algorithm determined that an outlier occurred. Each AP was independently tested 3 times, and 51 check results were obtained in total.

Fig. 10 shows the cumulative distribution function (CDF) of the ranging errors of the four APs. All APs had a ranging accuracy better than 1.35 m in 80% of the cases. However, the ranging errors could sometimes become large (4 m), especially for AP3 for which there was a serious NLOS between the transmitter and check point 7.

Fig. 11 provides the results of outlier detection. Both true outliers and detected outliers are marked. It can be seen that most outliers were correctly marked; however, a few missed detections and wrong detections also existed. Mistakes could occur more frequently when one distance was overestimated and another was underestimated. As shown in Table 1, the average outlier detection accuracy of the four APs was 85.3%, which proves that the proposed method can detect outliers to a large extent.

D. WI-FI FTM-BASED LOCALIZATION RESULTS AND ANALYSIS

In the third experiment, Wi-Fi FTM-based localization algorithms, which included the LS and proposed PF, were

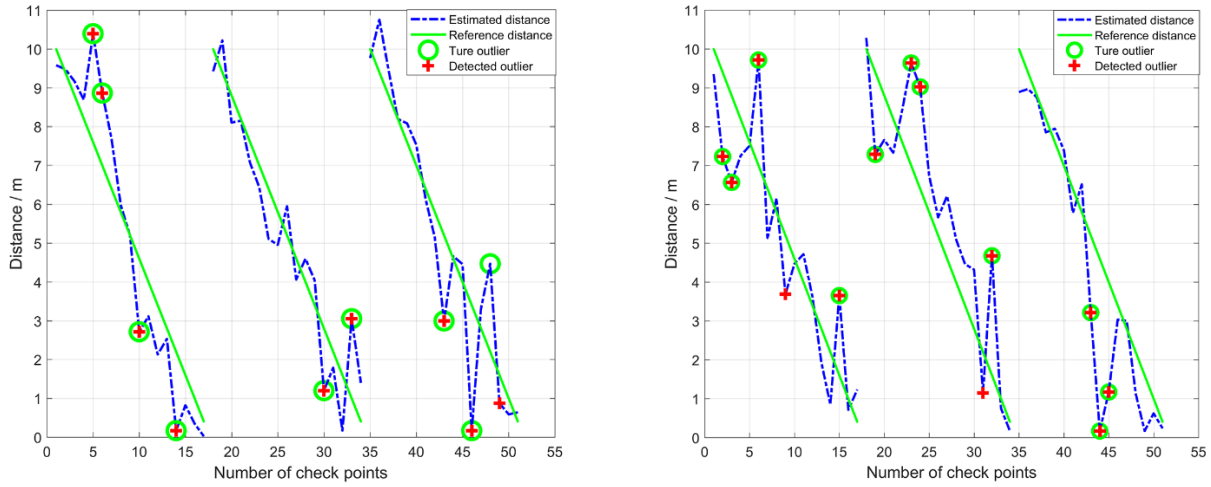

FIGURE 11. Outlier detection of AP1 and AP3. (a) AP1 with 51 checks. (b) AP3 with 51 checks.

TABLE 1. Comparison of positioning errors of different localization methods.

Number of AP	Check points	True outliers	Detected outliers	Miss detection	Wrong detection	Detected accuracy
1	51	9	9	1	1	77.8%
2	51	7	6	1	0	85.7%
3	51	11	13	0	2	81.9%
4	51	7	7	0	0	100.0%
Total	204	34	35	2	3	85.3%

compared under both static and dynamic modes. The particle number of the proposed PF was set to 2,000. All test data, including coordinate estimation and timestamp acquisition, were recorded in real time by the smartphone. In the static mode, the phone was placed on the first 9 check points at a height of 1.2 m in turn. Each point was tested for 2 minutes of data acquisition at a 1-Hz sampling rate. The measurements were compared with reference positions to calculate the errors. In the dynamic mode, the tester held the phone at a pitch of 30° and walked 6 laps each time with the different algorithms. The positioning errors were recorded whenever the tester passed through the check points. For each algorithm, 90 positioning errors were collected in total to compare and analyze with the others.

Since the locomotion activities were divided into static and dynamic modes, different experiment modes were designed. Fig. 12(a) and 12(b) depict the positioning errors of the x-axis and y-axis in the static mode, respectively. It is clear that the precision of the proposed PF is higher than that of the LS method at all check points and in both directions. In addition, the positioning errors of check points 7 and 8 are commonly greater than other points. This was because these two points behind the occlusion shown in Fig. 8 suffered a serious block of LOS, which led to poor accuracies.

Fig. 13 shows the performance of different localization algorithms in the dynamic mode. As seen from the figure, the PDR began to deviate from the reference

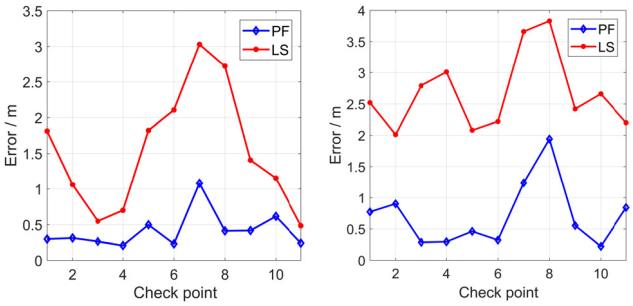

FIGURE 12. Positioning errors of the proposed PF and the LS method in static mode. (a) Positioning errors of the x-axis. (b) Positioning errors of the y-axis.

trajectory over time, and the LS had a poor accuracy without NLOS/multipath processing. The proposed PF had a better stability and higher positioning accuracy than the other algorithms.

Finally, the positioning errors of both the single source positioning methods and the proposed PF (2,000 particles) were compared in Table 2 and Fig. 14. As seen from this analysis, the proposed PF achieved an accuracy better than 1.2 m in 80% of the static cases and better than 1 m in 86.7% of the dynamic cases, whereas accuracies were better than 2 m and 3.4 m in 80% with PDR and LS, respectively. Based on the error statistics of Table 2, the proposed PF reduced

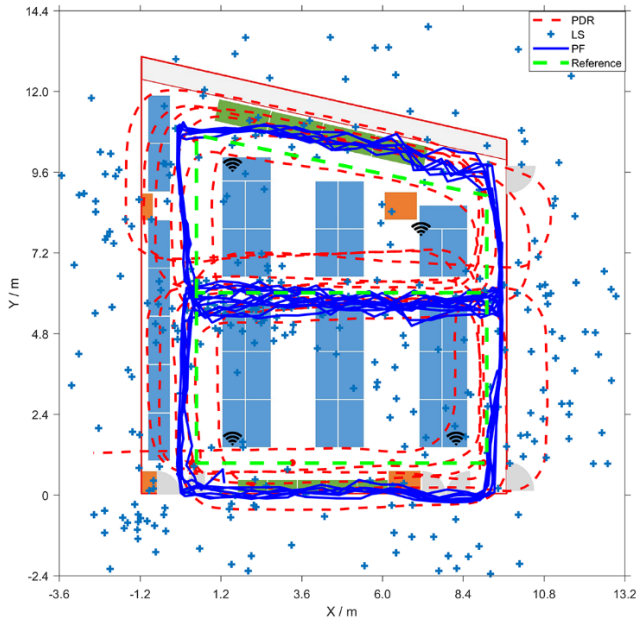

FIGURE 13. Comparison of different localization algorithms in pedestrian tracking.

TABLE 2. Comparison of positioning error statistics of different localization algorithms.

Method	Max error/m	Min error/m	Mean Error/m	Error variance
PDR (pitch=30°)	3.69	0.16	1.65	0.732
LS-static	6.62	0.14	2.21	1.740
PF-static	2.28	0.09	0.89	0.267
LS-dynamic	6.54	0.62	2.38	2.026
PF-dynamic	1.43	0.03	0.66	0.095

the error by approximately 59.7% and 72.3% under static and dynamic modes, respectively, compared with the Wi-Fi FTM-based LS method. The experimental results demonstrated that the performance of the proposed PF was not greatly affected by the deviation of PDR and the outliers of Wi-Fi FTM. In turn, the proposed PF could achieve a higher accuracy and stability.

E. COMPARISION OF THE PF USING DIFFERENT NUMBERS OF PARTICLES

In the last experiment, the performance of the proposed PF with different numbers of particles was displayed, and the calculation time and precision were compared. The system time of the smartphone in nanoseconds was recorded whenever a new PF output was obtained. The calculation time was defined as the difference between the two consecutive recorded system times, which included the Wi-Fi FTM reference time and the actual PF calculation time. Note that the reference time is larger than the defined sampling time (ideally 0.334 s but actually 0.4 s). Then, two groups of real-time data for 6 laps were collected that included heading, step length, Wi-Fi FTM ranging and timestamp. A simulation

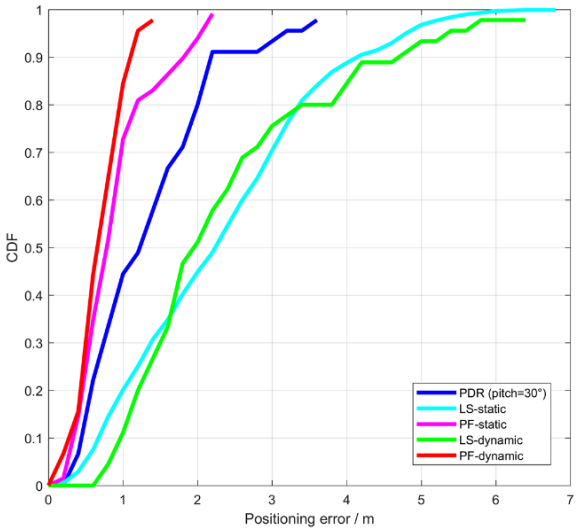

FIGURE 14. Comparison of positioning errors of different localization algorithms.

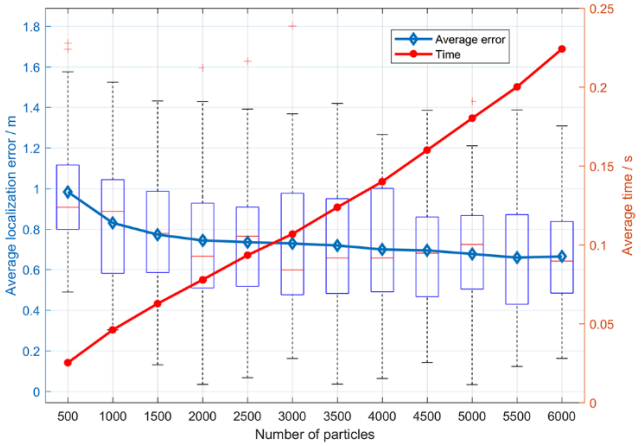

FIGURE 15. Comparison of localization errors and calculation time for different numbers of particles.

was performed to analyze the positioning accuracy of the proposed PF with different numbers of particles.

Fig. 15 describes the relationship between the simulated positioning errors and the average time of actual PF calculation with the number of particles increasing from 500 to 6,000. The figure shows that the average calculation time increased at a rate of 0.018 s per 500 particles. Assuming that the pedestrian walked with a step frequency of 2 Hz, the proposed PF with less than 3,000 particles could update the pedestrian's position in real time and sufficiently quickly that it obtained a new output within 0.5 s. On the other hand, the accuracy significantly improved when particle numbers went from 500 to 2,000; however, using more particles gave no noticeable improvement after convergence. We think that this is because 2,000 particles are sufficient to cover the entire interesting state-space area in this experimental site and that more particles may cause the probability distribution to be supersaturated.

V. CONCLUSIONS

In this paper, an enhanced particle filter algorithm was presented to fuse multi-sensors, Wi-Fi FTM, and map information. The PF algorithm was compared with single PDR and single FTM-based positioning methods. Adaptive tilt compensation was used to improve the conventional PDR; it helped to estimate precise headings when the smartphone pitch was from 0° to 90°, whereas the conventional PDR had a general error of 30°. Wi-Fi FTM is a new protocol and the LS method was used to calculate the positions. The performance of the proposed outlier detection resulted in an average precision of 85.3% over different APs. Finally, the proposed PF combined two different locomotion modes and intelligently monitored the particle set. The experiments indicated that the proposed PF with 2000 particles achieved a positioning accuracy of approximately 1 m under different modes and estimated a new position within 0.5 s. The algorithm improved the precision by approximately 59.7% and 72.3% under static and dynamic modes, respectively, compared with the Wi-Fi FTM-based LS method.

NLOS and multipath problems decreased the performance of localization. In this paper, no correction is adopted to filter-out the outliers, and the error would thus sometimes be relatively large. To reduce the negative impacts, effective solutions should be taken in the future. In addition, more detailed map information can be used to further improve the positioning accuracy of the particle filter.

REFERENCES

[1] R. Chen and L. Chen, "Indoor positioning with smartphones: The state-of-the-art and the challenges," *Acta Geod. Cartogr. Sin.*, vol. 46, pp. 1316–1326, 2017. doi: 10.11947/j.AGCS.2017.20170383.

[2] S. Feldmann, K. Kyamakya, A. Zapater, and Z. Lue, "An indoor bluetooth-based positioning system: Concept, implementation and experimental evaluation," in *Proc. Int. Conf. Wireless Netw.*, vol. 272, 2003, pp. 1–5.

[3] C. Yang and H.-R. Shao, "WiFi-based indoor positioning," *IEEE Commun. Mag.*, vol. 53, no. 3, pp. 150–157, Mar. 2015.

[4] M. Werner, M. Kessel, and C. Marouane, "Indoor positioning using smartphone camera," in *Proc. Int. Conf. Indoor Positioning Indoor Navigat.*, Guimaraes, Portugal, Sep. 2011, pp. 1–6.

[5] W. Kang and Y. Han, "SmartPDR: Smartphone-based pedestrian dead reckoning for indoor localization," *IEEE Sensors J.*, vol. 15, no. 5, pp. 2906–2916, May 2015.

[6] J. Liu, R. Chen, L. Pei, R. Guinness, and H. Kuusniemi, "A hybrid smartphone indoor positioning solution for mobile LBS," *Sensors*, vol. 12, no. 12, pp. 17208–17233, 2012.

[7] G. Guo, R. Chen, F. Ye, L. Chen, Y. Pan, M. Liu, and Z. Cao, "A pose awareness solution for estimating pedestrian walking speed," *Remote Sens.*, vol. 11, no. 1, p. 55, 2019.

[8] R. M. Faragher, C. Sarno, and M. Newman, "Opportunistic radio SLAM for indoor navigation using smartphone sensors," in *Proc. IEEE/ION Position, Location Navigat. Symp.*, Myrtle Beach, SC, USA, Apr. 2012, pp. 120–128.

[9] R. Chen, W. Chen, X. Chen, X. Zhang, and Y. Chen, "Sensing strides using EMG signal for pedestrian navigation," *GPS Solutions*, vol. 15, no. 2, pp. 161–170, Apr. 2011.

[10] C. Huang, Z. Liao, and L. Zhao, "Synergism of INS and PDR in self-contained pedestrian tracking with a miniature sensor module," *IEEE Sensors J.*, vol. 10, no. 8, pp. 1349–1359, Aug. 2010.

[11] J. Cheon, H. Hwang, D. Kim, and Y. Jung, "IEEE 802.15.4 ZigBee-based time-of-arrival estimation for wireless sensor networks," *Sensors*, vol. 16, no. 2, p. 203, 2016. doi: 10.3390/s16020203.

[12] M. Youssef and A. Agrawala, "The horus WLAN location determination system," in *Proc. 3rd Int. Conf. Mobile Syst., Appl., Services*, 2005, pp. 205–218.

[13] Z. Yang, Z. Zhou, and Y. Liu, "From RSSI to CSI: Indoor localization via channel response," *ACM Comput. Surv.*, vol. 46, no. 2, pp. 25:1–25:32, Dec. 2013.

[14] F. Evennou and F. Marx, "Advanced integration of WiFi and inertial navigation systems for indoor mobile positioning," *EURASIP J. Adv. Signal Process.*, vol. 2006, Dec. 2006, Art. no. 086706.

[15] G. Chen, X. Meng, Y. Wang, Y. Zhang, P. Tian, and H. Yang, "Integrated WiFi/PDR/smartphone using an unscented Kalman filter algorithm for 3D indoor localization," *Sensors*, vol. 15, no. 9, pp. 24595–24614, 2015.

[16] L. Banin, U. Schatzberg, and Y. Amizur, "Next generation indoor positioning system based on WiFi time of flight," in *Proc. 26th Int. Tech. Meeting Satell. Division Inst. Navigat. (ION GNSS)*, 2013, pp. 975–982.

[17] U. Schatzberg, L. Banin, and Y. Amizur, "Enhanced WiFi ToF indoor positioning system with MEMS-based INS and pedometric information," in *Proc. IEEE/ION Position, Location Navigat. Symp. (PLANS)*, Monterey, CA, USA, May 2014, pp. 185–192.

[18] *IEEE Standard for Information Technology—Telecommunications and Information Exchange Between Systems Local and Metropolitan Area Networks–Specific Requirements—Part 11: Wireless LAN Medium Access Control (MAC) and Physical Layer (PHY) Specifications*, IEEE Standard 802.11-2016 and 802.11-2012, Dec. 2016.

[19] L. Banin, U. Schatzberg, and Y. Amizur, "WiFi FTM and map information fusion for accurate positioning," in *Proc. Int. Conf. Indoor Positioning Indoor Navigat. (IPIN)*, 2016, pp. 1–4.

[20] M. Ibrahim, H. Liu, M. Jawahar, V. Nguyen, M. Gruteser, R. Howard, B. Yu, and F. Bai, "Verification: Accuracy evaluation of WiFi fine time measurements on an open platform," in *Proc. 24th Annu. Int. Conf. Mobile Comput. Netw.*, 2018, pp. 417–427.

[21] *Wi-Fi Location: Ranging With RTT | Android Developers*. Accessed: 2019. [Online]. Available: https://developer.android.com/guide/topics/connectivity/wifi-rtt.html

[22] L. Wang, R. Chen, L. Chen, L. Shen, P. Zhang, Y. Pan, and M. Li, "A robust filter for TOA based indoor localization in mixed LOS/NLOS environment," in *Proc. Ubiquitous Positioning, Indoor Navigat. Location-Based Services (UPINLBS)*, Wuhan, China, Mar. 2018, pp. 1–9.

[23] L. Banin, O. Bar-Shalom, N. Dvorecki, and Y. Amizur. *High-Accuracy Indoor Geolocation Using Collaborative Time of Arrival*. Accessed: 2019. [Online]. Available: https://www.researchgate.net/publication/320146822

[24] L. Banin, O. Bar-Shalom, N. Dvorecki, and Y. Amizur, "Scalable Wi-Fi client self-positioning using cooperative FTM-sensors," *IEEE Trans. Instrum. Meas.*, to be published.

[25] Y. Yu, R. Chen, L. Chen, G. Guo, F. Ye, and Z. Liu, "A robust dead reckoning algorithm based on Wi-Fi FTM and multiple sensors," *Remote Sens.*, vol. 11, no. 5, p. 504, 2019.

[26] R. Chen, T. Chu, K. Liu, J. Liu, and Y. Chen, "Inferring human activity in mobile devices by computing multiple contexts," *Sensors*, vol. 15, no. 9, pp. 21219–21238, 2015.

[27] Z. Khan, T. Balch, and F. Dellaert, "MCMC-based particle filtering for tracking a variable number of interacting targets," *IEEE Trans. Pattern Anal. Mach. Intell.*, vol. 27, no. 11, pp. 1805–1819, Nov. 2005.

[28] H. Nurminen, A. Ristimäki, S. Ali-Löytty, and R. Piché, "Particle filter and smoother for indoor localization," in *Proc. Int. Conf. Indoor Positioning Indoor Navigat., Montbeliard-Belfort*, Oct. 2013, pp. 1–10.

[29] N. Dvorecki, O. Bar-Shalom, L. Banin, and Y. Amizur, "A machine learning approach for Wi-Fi RTT ranging," in *Proc. Int. Tech. Meeting Inst. Navigat.*, Reston, VA, USA, Jan. 2019, pp. 435–444.

[30] U. Niesen, V. N. Ekambaram, J. Jose, and X. Wu, "Intervehicle range estimation from periodic broadcasts," *IEEE Trans. Veh. Technol.*, vol. 66, no. 12, pp. 10637–10646, Dec. 2017.

[31] N. Alessandro, S. Pietro, M. Massimo, and R. Francesco, "Indoor vehicle localization based on Wi-Fi navigation beacons for multi-modal transportation applications," in *Proc. ION Pacific PNT Meeting*, Honolulu, HI, USA, Apr. 2019, pp. 493–506.

[32] L. Fang, P. J. Antsaklis, L. A. Montestruque, M. B. McMickell, M. Lemmon, Y. Sun, H. Fang, P. J. Antsaklis, L. A. Montestruque, M. B. McMickell, M. Lemmon, Y. Sun, H. Fang, I. Koutroulis, M. Haenggi, M. Xie, and X. Xie, "Design of a wireless assisted pedestrian dead reckoning system—The NavMote experience," *IEEE Trans. Instrum. Meas.*, vol. 54, no. 6, pp. 2342–2358, Dec. 2005.

[33] S. Beauregard and H. Haas, "Pedestrian dead reckoning: A basis for personal positioning," in *Proc. 3rd Workshop Positioning, Navigat. Commun.*, 2006, pp. 27–35.
[34] Z. Tian, Y. Zhang, M. Zhou, and Y. Liu, "Pedestrian dead reckoning for MARG navigation using a smartphone," *EURASIP J. Adv. Signal Process.*, vol. 2014, no. 1, p. 65, 2014.
[35] R. Chen, L. Pei, and Y. Chen, "A smart phone based PDR solution for indoor navigation," in *Proc. 24th Int. Tech. Meeting Satell. Division Inst. Navigat.*, 2011, pp. 1404–1408.
[36] F. Li, C. Zhao, G. Ding, J. Gong, C. Liu, and F. Zhao, "A reliable and accurate indoor localization method using phone inertial sensors," in *Proc. ACM Conf. Ubiquitous Comput.*, 2012, pp. 421–430.
[37] V. Renaudin, C. Combettes, and F. Peyret, "Quaternion based heading estimation with handheld MEMS in indoor environments," in *Proc. IEEE/ION Position, Location Navigat. Symp. (PLANS)*, Monterey, CA, USA, May 2014, pp. 645–656.
[38] W. Premerlani and P. Bizard. *Direction Cosine Matrix IMU: Theory*. [Online]. Available: https://www.researchgate.net/publication/265755808.
[39] S. Ayub, A. Bahraminasab, and B. Honary, "A sensor fusion method for smart phone orientation estimation," in *Proc. 13th Annu. Post Graduate Symp. Converg. Telecommun., Netw. Broadcast.*, Liverpool, U.K., Jun. 2012.
[40] X. Yun and E. R. Bachmann, "Design, implementation, and experimental results of a quaternion-based Kalman filter for human body motion tracking," *IEEE Trans. Robot.*, vol. 22, no. 6, pp. 1216–1227, Dec. 2006.
[41] D. Choukroun, I. Bar-Itzhack, and Y. Oshman, "Novel quaternion Kalman filter," *IEEE Trans. Aerosp. Electron. Syst.*, vol. 42, no. 1, pp. 174–190, Jan. 2006.
[42] J. Menke and A. Zakhor, "Multi-modal indoor positioning of mobile devices," in *Proc. Int. Conf. Indoor Positioning Indoor Navigat. (IPIN)*, Banff, AB, Canada, 2015, pp. 1–4.
[43] S. Wang, K. Liu, Y. Liu, and X. Sun, "Analysis for low cost inertial sensors based pedestrian dead reckoning," in *Proc. 2nd Int. Conf. Commun., Signal Process., Syst.* Cham, Switzerland: Springer, 2014, pp. 1029–1037.
[44] *SensorManager | Android Developers*. Accessed: 2019. [Online]. Available: https://developer.android.com/reference/android/hardware/SensorManager.html
[45] F. Gustafsson, "Particle filter theory and practice with positioning applications," *IEEE Aerosp. Electron. Syst. Mag.*, vol. 25, no. 7, pp. 53–82, Jul. 2010.
[46] M. S. Arulampalam, S. Maskell, N. Gordon, and T. Clapp, "A tutorial on particle filters for online nonlinear/non-Gaussian Bayesian tracking," *IEEE Trans. Signal Process.*, vol. 50, no. 2, pp. 174–188, Feb. 2002.
[47] J. M. Pak, C. K. Ahn, Y. S. Shmaliy, and M. T. Lim, "Improving reliability of particle filter-based localization in wireless sensor networks via hybrid particle/FIR filtering," *IEEE Trans. Ind. Informat.*, vol. 11, no. 5, pp. 1089–1098, Oct. 2015.
[48] S. Beauregard, Widyawan, and M. Klepal, "Indoor PDR performance enhancement using minimal map information and particle filters," in *Proc. IEEE/ION Position, Location Navigat. Symp.*, Monterey, CA, USA, May 2008, pp. 141–147.
[49] P. Blanchart, L. He, and F. Le Gland, "Information fusion for indoor localization," in *Proc. 12th Int. Conf. Inf. Fusion*, Seattle, WA, USA, Jul. 2009, pp. 2083–2090.
[50] H. Nurminen, M. Raitoharju, and R. Pichè, "An efficient indoor positioning particle filter using a floor-plan based proposal distribution," in *Proc. 19th Int. Conf. Inf. Fusion (FUSION)*, Berlin, Germany, Jul. 2016, pp. 541–548.
[51] B. Turgut and R. P. Martin, "Restarting particle filters: An approach to improve the performance of dynamic indoor localization," in *Proc. IEEE Global Telecommun. Conf. (GLOBECOM)*, Honolulu, HI, USA, Nov./Dec. 2009, pp. 1–7.
[52] T.-C. Li, G. Villarrubia, S.-D. Sun, J. M. Corchado, and J. Bajo, "Resampling methods for particle filtering: Identical distribution, a new method, and comparable study," *Frontiers Inf. Technol. Elect. Eng.*, vol. 16, no. 11, pp. 969–984, 2015.

SHIHAO XU received the B.S. degree in surveying and mapping engineering from the China University of Mining and Technology, Jiangsu, China. He is currently pursuing the M.S. degree in geodesy and survey engineering with Wuhan University, Wuhan, China. His research interests include the development of location-based services, indoor positioning and navigation technology, and information fusion.

RUIZHI CHEN is currently a Professor and the Director of the State Key Laboratory of Information Engineering in surveying, mapping, and remote sensing with Wuhan University. He was an Endowed Chair Professor with Texas A&M University Corpus Christi, USA, the Head and a Professor of the Department of Navigation and Positioning, Finnish Geodetic Institute, Finland, and the Engineering Manager of Nokia, Finland. He has published two books and more than 200 scientific papers. His current research interests include indoor positioning, satellite navigation, and location-based services.

YUE YU received the B.S. and M.S. degrees from the Chongqing University of Posts and Telecommunications. He is currently pursuing the Ph.D. degree in geodesy and survey engineering with Wuhan University, China. His research interests include the inertial positioning and navigation technology, indoor positioning and navigation technology based on chance signal and signal processing, and fusion technology.

GUANGYI GUO received the B.S. and M.S. degrees in geographic information science from Hubei University, Hubei, China, in 2012 and 2015, respectively. He is currently pursuing the Ph.D. degree in cartology and geographical information science with Wuhan University, Wuhan, China. His research interests include indoor positioning, machine learning, and the Internet of Things.

LIXIONG HUANG is currently pursuing the B.S. degree in geodesy and geomatics engineering from Wuhan University, Hubei, China. He will pursue the master's degree with Wuhan University. His research interests include indoor positioning, the Internet of Things, and information fusion.